DOI: 10.1002/ ((please add manuscript number))
Article type: (**Full Paper**)

Bioorthogonal Photo-Catalytic Activation of an Anti-Cancer Prodrug by Riboflavin

Xin Yang[+], Limin Ma[+], Hongwei Shao[+], Xia Ling, Mengyu Yao, Guowen Luo, Stefano Scoditti, Emilia Sicilia, Gloria Mazzone,* Meng Gao,* and Ben Zhong Tang**

X. Yang, X. Ling, Prof. M. Gao
National Engineering Research Center for Tissue Restoration and Reconstruction, Key Laboratory of Biomedical Engineering of Guangdong Province, Key Laboratory of Biomedical Materials and Engineering of the Ministry of Education, Innovation Center for Tissue Restoration and Reconstruction, South China University of Technology, Guangzhou 510006, China
E-mail: msmgao@scut.edu.cn
H. Shao, M. Yao, G. Luo, Prof. L. Ma
Department of Orthopedics, Guangdong Provincial People's Hospital, Guangdong Academy of Medical Sciences, Guangzhou, Guangdong, 510080, China
E-mail: malimin7@126.com
S. Scoditti, Prof. E. Sicilia, Prof. G. Mazzone
Department of Chemistry and Chemical Technologies, Università della Calabria, 87036 Arcavacata di Rende, CS, Italy.
E-mail: gloria.mazzone@unical.it
Prof. B. Z. Tang
AIE institute, State Key Laboratory of Luminescent Materials and Devices, Center for Aggregation-Induced Emission, Guangdong Provincial Key Laboratory of Luminescence from Molecular Aggregates, Guangzhou International Campus, South China University of Technology, Guangzhou 510640; Shenzhen Institute of Aggregate Science and Technology, School of Science and Engineering, The Chinese University of Hong Kong, Shenzhen 518172, China
E-mail: tangbenz@cuhk.edu.cn
[+] These authors contributed equally to this work.

Keyword: biorthogonal photocatalysis; prodrug; cancer; riboflavin; fluorescence

Abstract

Chemotherapies for cancer treatment usually suffer from poor targeting ability and serious side-effects. To improve the treatment efficiency and reduce side effects, photoactivatable chemotherapy has been recently proposed for precise cancer treatment with high spatiotemporal resolution. However, most photoactivatable prodrugs require decoration by stoichiometric photo-cleavable groups, which are only responsive to ultraviolet irradiation and suffer from low reaction efficiency. To tackle these challenges, we herein propose a bioorthogonal photo-catalytic activation strategy with riboflavin as the catalyst for *in situ* transformation of prodrug dihydrochelerythrine (DHCHE) prodrug into anti-cancer drug chelerythrine (CHE), which can efficiently kill cancer cells and inhibit *in vivo* tumor growth under light irradiation. Meanwhile, the photo-catalytic transformation from DHCHE into CHE was *in situ* monitored by green-to-red fluorescence conversion, which can be used for precise control of the therapeutic dose. The photocatalytic mechanism was also fully explored by means of density functional theory (DFT) calculations. We believe this imaging-guided bioorthogonal photo-catalytic activation strategy is promising for cancer chemotherapy in clinical applications.

1. Introduction

Chemotherapy usually suffers from serious side-effects due to the off-target toxicity.[1] Therefore, it's highly desirable for precise activation of chemotherapy at tumor sites to improve treatment efficiency and reduce side effects. To achieve precise cancer treatment, various external stimuli-responsive strategies have been proposed for *in situ* activation of prodrugs, such as pH, enzymes and photoirradiation.[2] Among these methods, the photoactivation strategy is featured with the significant advantage of high spatiotemporal resolution and is especially suitable for treatment of shallow-seated tumors.[3] However, conventional photoactivatable chemotherapy usually requires decoration of chemotherapeutics with stoichiometric photo-responsive groups,[4] which not only require

tedious synthetic procedures for preparation, but also suffer from low photoactivation efficiency and easy generation of toxic byproducts. Moreover, most of current photo-responsive groups are only responsive to cytotoxic ultraviolet (UV) irradiation with low absorption coefficients, which seriously restrict their *in vivo* applications.[4c]

Recently, photocatalytic activation of chemotherapeutics has been proposed to greatly improve the chemotherapy efficiency.[5] Compared with metal catalysts, biogenic organic photocatalysts are more attractive for *in vivo* applications with excellent biocompatibility.[6] For example, riboflavin (Rf) as the precursor of flavin cofactors has been used for the activation of Pt^{IV} and Ru^{IV} prodrugs via photo-reduction reactions.[7-8] Herein, based on our previous study of photoactivatable imaging and cancer therapies,[9] we proposed a biorthogonal photocatalytic strategy with riboflavin as the photocatalyst for *in situ* activation of the non-toxic prodrug dihydrochelerythrine (DHCHE) into anticancer drug chelerythrine (CHE) under white light or blue light irradiation. The photocatalytic mechanism was fully explored by means of density functional theory (DFT) calculations. With A375 cancer cells and melanoma tumor bearing mice as a model, the combination of "DHCHE + Rf" under light irradiation showed a high efficiency for killing of cancer cells and inhibition of *in vivo* tumor growth. Meanwhile, the photocatalytic activation from DHCHE into CHE can be *in situ* monitored by green-to-red fluorescence conversion, which can be used for precise control of the therapeutic dose.

2. Results and Discussion

2.1 Photocatalytic transformation from DHCHE into CHE

With DHCHE as the prodrug, we first screened a series of photocatalysts to promote its transformation into anticancer drug CHE, including $[Ru(bpy)_3]^{2+}$, tetraphenylporphyrin, Al(III) phthalocyanine chloride tetrasulfonic acid, hemin, methylene blue, rose bengal, 9-mesityl-10-methylacridinium perchlorate and riboflavin (**Figure S1**, Supporting Information). Among these photocatalysts, only riboflavin can efficiently promote the transformation from

DHCHE into CHE, which was verified by UV-Vis absorption and HPLC spectra measurement (**Figure 1**B-D). As shown in **Figure 1**C, for "DHCHE (100 μM) + Rf (50 μM)" in aqueous solution under white light irradiation (34 mW cm^{-2}), the absorption intensities at 266 nm and 318 nm gradually increased, which can be ascribed to the generation of CHE. The conversion efficiency from DHCHE to CHE also increased with the increasing Rf concentration, which was verified by the absorbance spectra measurement (**Figure S2**, Supporting Information). The photocatalytic transformation from DHCHE into CHE was also verified by HPLC spectra measurement. For "DHCHE (0.5 mg mL^{-1}) + Rf (0.05 mg mL^{-1})" under blue light irradiation (500 nm, 50 mW cm^{-2}) for 30 min, the integration value of DHCHE peak decreased from 95.7% to 5.3%, while the integration value of CHE peak increased from 0.4% to 70.1% (**Figure 1**E, **Figure S3**, Supporting Information). Interestingly, a faster transformation from DHCHE into CHE was observed in weakly acidic solution (pH = 6) than in neutral or weakly basic solution (pH = 7 or 8) (**Figure S4**, Supporting Information), which suggests the combination of "DHCHE + Rf" under light irradiation is especially suitable for photoactivatable treatment of tumor with a weakly acidic environment (pH ~6).[10]

2.2 Photocatalytic mechanism

Computational approaches were exploited to shed light on the photocatalytic mechanism of DHCHE conversion to CHE by Rf. A possible photocatalytic reaction mechanism was proposed in **Scheme 2**. Upon light irradiation, Rf singlet exited state can undergo intersystem crossing (ISC) to triplet state $^3Rf^*$ and then react with DHCHE via an electron transfer process to afford $Rf^{\bullet-}$ and $DHCHE^{\bullet+}$, which then undergo hydrogen abstraction reaction to yield HRf^- and CHE. The HRf^- intermediate can be oxidized by oxygen to regenerate Rf (**Figure S5**, Supporting Information).[11] In order to verify that the excited triplet state $^3Rf^*$ as an electron acceptor is critical to promote the transformation from DHCHE into CHE, Trolox was used as an electron donor to quench $^3Rf^*$ and the photocatalytic transformation was efficiently

inhibited (**Figure S6**, Supporting Information).[12] Moreover, the low oxidation potential of DHCHE (E_{ox} = 0.25 V) suggests that it can be easily oxidized by $^3Rf^*$ (E_{ox} = 1.77 V) via photoinduced electron transfer process (**Figure S7**, Supporting Information).[13]

The computational exploration of the photophysical Rf properties confirms that it can be excited under blue light irradiation causing a π→π* transition (as evidenced by HOMO and LUMO plots in **Figure 2**A) and then an intersystem spin crossing from the bright state to the triplet manifold can occur. Indeed, the spin-orbit coupling values, accounting for ISC kinetics, suggest the viability of a preferential ISC channel $S_1 \rightarrow T_1$ (SOC = 14.2 cm^{-1}), here labelled as $^3Rf^*$.

To further ascertain that an electron transfer from DHCHE to $^3Rf^*$ could occur and to evaluate the energy gain of this process, the computation of radical anion and cation of Rf and DHCHE energies, respectively, were taken into consideration. With respect to the reactants' energy sum ($^3Rf^*$ + DHCHE), the electron shift for $Rf^{\bullet-}$ and $DHCHE^{\bullet+}$ formation entails an energy gain of 12.9 kcal mol^{-1}. Therefore, once Rf is excited and the $^3Rf^*$ triplet state results populated, an electron is transferred from DHCHE to $^3Rf^*$ to afford $Rf^{\bullet-}$ and $DHCHE^{\bullet+}$. From here, for the sake of comparison and to prove that the subsequent hydrogen abstraction from DHCHE by Rf is facilitated when the Rf in its triplet state is involved in the reaction mechanism, such step was explored even along the ground state singlet energy surface (black line in **Figure 2**B). In both spin multiplicities, the initial (Rf···DHCHE) is characterized by a π-π stacking interaction (**Figure S8**A, Supporting Information) and is stabilized of 25.5 and 10.3 kcal mol^{-1} along the triplet and singlet energy surfaces, respectively with respect to the corresponding reference energies of separated reactants.

The analysis of the spin density of $Rf^{\bullet-}$····$DHCHE^{\bullet+}$ confirms the localization of the unpaired electrons on the key N atoms of Rf and DHCHE (**Figure S8**B, Supporting Information), as sketched in **Scheme 2**, accessible only along the triplet state energy surface. The hydrogen abstraction occurs through the transition state labelled TS_H in which the

hydrogen atom is almost transferred from the C atom of DHCHE to the N atom of Rf (**Figure S8**C, Supporting Information). The energy barrier to be overcome to yield HRf^- and CHE is significantly lower along the triplet surface than the singlet one (6.6 *vs* 21 kcal mol^{-1}). Along the triplet free energy profile such a transfer is realized by a hydrogen atom (H·) migration starting from the $Rf^{\bullet-}\cdots DHCHE^{\bullet+}$ adduct in which the two unpaired electrons are localized separately on the two reactants, whereas along the singlet surface a hydride migration should occur. Along the kinetically favoured pathway (red line in **Figure 2**B) the whole reaction results only slightly endergonic. Therefore, it is reasonable to hypothesize that the reaction should be favoured if Rf is first excited and then reacts with DHCHE to afford the anticancer drug CHE.

The free energy surface describing a plausible restoring of Rf by molecular oxygen naturally present in the environment is reported in **Figure 2**C. At physiological pH, it can be hypothesized that the HRf^- species, formed according to the photocatalytic mechanism described above, is converted into its di-protonated form H_2Rf depicted in **Scheme 2**. Thus, the reaction between H_2Rf and O_2 leading to the formation of Rf and H_2O_2 was explored and the optimized structures of the intercepted stationary points are reported in **Figure S9**. As one of the reactants, molecular oxygen, is in its ground triplet state the reaction mechanism surely starts in triplet state. Along such free energy profile, the reaction passes through two transition state that require substantially different amounts of energy to be overcome. The first H-abstraction occurs overcoming an energy barrier of only 5.7 kcal mol^{-1} and the formed product, that is the adduct between HRf and OOH (HRf···OOH), lies 3.1 kcal mol^{-1} above the reference. The subsequent H abstraction requires the overcoming of an energy barrier five times higher than the first one. However, the final product, that is the adduct between the restored Rf and the H_2O_2, results much more stable along the singlet free energy surface (green line in **Figure 2**C). As a consequence, a spin crossing from the triplet to the singlet spin surface has to occur. In addition, all the numerous attempts carried out to locate a

transition state for the second hydrogen transfer along such surface failed, meaning that when the OOH moiety comes close to the NH site it is rapidly converted into H_2O_2 and the Rf is thus restored.

2.3 Cancer Cell Imaging and Killing

We then investigated the cancer cell imaging and killing ability of "Rf + DHCHE" with melanoma A375 cells as a model. For cells treated with "DHCHE (50 μM) + Rf (10 μM)" under white light irradiation (34 mW cm^{-2}) for only 1.0 min, an obviously turn-on red fluorescence in nucleus and a decreased green fluorescence in cytoplasm was observed under confocal laser scanning microscope (CLSM) (**Figure 3**A-B). In contrast, only a green fluorescence was observed in cytoplasm for treatment with only DHCHE (50 μM) under light irradiation. These results suggest that Rf as a photocatalyst can efficiently promote the intramolecular transformation of green-emissive DHCHE in cytoplasm into red-emissive CHE with nucleus targeting ability.

The cancer cell killing ability of "Rf + DHCHE" was then investigated via MTT assay. The cancer cell viability decreased to almost zero by treatment with "DHCHE (20 μM) + Rf (5 μM)" under white light irradiation (34 mW cm^{-2}) for 10 min (**Figure 3**E-F). In contrast, a high cell viability (>60%) was observed for treatment with only DHCHE (20 μM) or Rf (20 μM) (**Figure 3**C-D). These results suggest that the fast transformation from DHCHE into CHE catalyzed by Rf can efficiently kill cancer cells (**Figure S10**, Supporting Information).

The Annexin V-FITC/propidium iodide (PI) assay was then conducted for monitoring of cell apoptosis induced by "DHCHE + Rf" under light irradiation (+ L). The A375 cells were first treated with "DHCHE(50 μM) + Rf (10 μM)" for 30 min and then irradiated by white light (34 mW cm^{-2}) for 10 min, the cytoplasm and nucleus were respectively stained with Annexin V-FITC/PI, which suggests "DHCHE + Rf (+ L)" can efficiently induce cancer cell apoptosis (**Figure 4**A). The flow cytometry analysis was also conducted and a much higher apoptotic ratio (61.40%) was observed for "DHCHE + Rf (+ L)" group than the other groups,

such as “DHCHE (+ L)” (12.95%) and “Rf (+ L)” (12.86%) (**Figure 4**B). The apoptosis mechanism was then investigated via quantitative reverse transcription PCR (qRT-PCR) analysis. A significantly higher expression of pro-apoptotic genes (Bax, P53 and Caspase-3) and a lower expression of anti-apoptotic gene (Bcl2) were observed for the “DHCHE + Rf (+ L)” group than the other groups (**Figure 4**C-D, **Table S1**, Supporting Information). The apoptosis-inducing ability of “DHCHE + Rf (+ L)” can be ascribed to the efficient transformation into cytotoxic CHE associating with generation of many reactive oxygen species (ROS) (**Figure S11-S13**, Supporting Information).[14]

2.4 Inhibition of Tumor Growth

The *in vivo* tumor inhibition experiment was performed with melanoma A375-bearing nude mice as a model, which were randomly divided into seven groups: Control, DHCHE, DHCHE (+ L), Rf, Rf (+ L), “DHCHE + Rf”, and “DHCHE + Rf (+ L)”. Different groups were treated with the corresponding agents every 2 days by intertumoral injection. For light irradiation (+ L) groups, the mice were irradiated under blue light irradiation (500 nm, 50 mW cm^{-2}) for 30 min after intertumoral injection of therapeutic agents. As shown in **Figure 5**B, the body weight of mice did not show obvious decrease for all groups after treatment for 14 days, whereas the tumor volume and weight of “DHCHE + Rf (+ L)” group was much lower than the other groups (**Figure 5**C-D). The tumors were then dissected and analyzed by hematoxylin and eosin (H&E) and immunohistochemical staining (**Figure 5**E). For the “DHCHE + Rf (+ L)” group, an obviously increased vacuole and condensed nuclei were observed. It also showed the highest expression of pro-apoptotic Caspace-3 and lowest expression of anti-apoptotic Ki-67 among the treatment groups (**Figure 5**F). These results suggest that the tumor growth can be efficiently inhibited by “DHCHE + Rf (+ L)”.

2.5 *In Vivo* Biosafety Evaluation

In order to evaluate the biosafety, major organs were collected and analyzed by H&E staining after treatment for 14 days. Compared with healthy nude mice (blank group) and control

group treated with physiological saline, the "DHCHE + Rf (+ L)" group did not show obvious inflammation lesions or impairment (**Figure 6**A). Meanwhile, the expression level of blood indicators were comparable for different treatment groups, including blood urea nitrogen (BUN), alanine aminotransferase (ALT), aspartate aminotransferase (AST) and total protein (TP). These results suggest that "DHCHE + Rf (+ L)" has an excellent biocompatibility (**Figure 6**B-E).

3. Conclusion

In conclusion, we proposed a photocatalytic activation strategy for *in situ* and fast transformation of DHCHE into anticancer-active CHE with Rf as the bioorthogonal photocatalyst, which showed a high efficiency for inducing cancer cell apoptosis *in vitro* and inhibition of tumor growth *in vivo*. Meanwhile, the photocatalytic activation process can be *in situ* monitored by fluorescence imaging, which can be used for precise control of the therapeutic dose. We believe this biorthogonal photocatalytic activation strategy for chemotherapy is promising for precise cancer treatment.

4. Experimental Section

Cell Imaging: The A375 cells in culture media were first treated with "DHCHE (50 μM) + Rf (10 μM)" or DHCHE (50 μM) for 30 min, and then the cells were irradiated under white light irradiation (34 mW cm^{-2}) for different time. The CLSM images were then taken under confocal microscope. For DHCHE (green channel), λ_{ex} = 405 nm, λ_{em} = 420-520 nm. For CHE (red channel), λ_{ex} = 488 nm, λ_{em} = 580-700 nm. Scale bar = 20 μm.

Apoptosis In Situ Monitored by CLSM: The A375 cells in culture media were first treated with "DHCHE (50 μM) + Rf (10 μM)" for 30 min and further treated with Annexin V-FITC/PI for 10 min, then the cells were irradiated under white light irradiation (34 mW cm^{-2}) for different time. The CLSM images were then taken under confocal microscope. For DHCHE, λ_{ex} = 405 nm, λ_{em} = 420-520 nm. For CHE, λ_{ex} = 488 nm, λ_{em} = 580-700 nm. For Annexin V-FITC, λ_{ex} = 488 nm, λ_{em} = 510-550 nm. For PI, λ_{ex} = 543 nm, λ_{em} = 560-625 nm. Scale bar = 20 μm.

Apoptosis Analyzed by Flow Cytometry: The A375 cells were seeded into six-well plates (2.5 × 10^5 cells/well) for 24 h. After incubation of cells with different therapeutic agents for 30 min, including "DHCHE (20 μM) + Rf (10 μM)", DHCHE (20 μM) and Rf (10 μM), the cells were further irradiated under white light irradiation (34 mW cm^{-2}) for 10 min. After further incubation at 37 °C for 24 h, the cells were collected and treated with Annexin V-FITC/PI for 15 min. The percentage of apoptotic ratio was then analyzed by flow cytometry.

In Vivo Tumor Therapy: All mice experiments were approved by Animal Center of South China University of Technology and were performed in compliance with the Regulation on the Administration of Laboratory Animals established by the State Council, the People's Republic of China. Briefly, A375 cells (2 × 10^6) were subcutaneous injected into right back positions to establish the tumor model of Balb/c nude mice. When the tumor volume reached approximately 200 mm^3, the mice were randomly divided into seven groups: control group (PBS), DHCHE (2.0 mg kg^{-1}), DHCHE (+ L) group (2.0 mg kg^{-1}), Rf group (1.0 mg kg^{-1}), Rf (+ L) group (1.0 mg kg^{-1}), "DHCHE + Rf "group (2.0 mg kg^{-1} DHCHE and 1.0 mg kg^{-1} Rf), "DHCHE + Rf (+ L)"group (2.0 mg kg^{-1} DHCHE and 1.0 mg kg^{-1} Rf) (n = 5 for each group). The mice were treated with corresponding therapeutic agents every 2 days by intratumoral injection and the tumor region was irradiated with 500 nm light (50 mW cm^{-2}, 30 min). During the treatment period, the tumor volume of all mice was measured every 2 days using a vernier caliper (tumor volume $V = L * W^2/2$, L is tumor length and W is tumor wide). After treatment for 14 days, all the mice were sacrificed and the major organs and tumors collected from the bodies were analyzed by H&E and immunohistochemical staining.

Supporting Information

Supporting Information is available from the Wiley Online Library or from the author.

Acknowledgements

This work was financially supported by the National Science Foundation of China (21788102, 51620105009, 22175065, 21877040, U1801252); the National Key R&D Program of China (2018YFC0311103); the Science and Technology Planning Project of Guangzhou (201804020060, 202007020002 and 201607020015); Natural Science Foundation of Guangdong Province (2020B1515020010, 2020A1515110746, 2020B0101030006 and 2020A1515010827); the High-level Hospital Construction Project (KJ012019100); the University of Calabria and Calabria Region (project POR Calabria–FSE/FESR 2014-2020) for financial support.

Conflict of Interest

The authors declare no conflict of interest.

References

[1] a) M. Gao, B. Z. Tang, *Coord. Chem. Rev.* **2020**, *402*, 213076; b) W. Liu, X. Luo, Y. Bao, Y. P. Liu, G. H. Ning, I. Abdelwahab, L. Li, C. T. Nai, Z. G. Hu, D. Zhao, B. Liu, S. Y. Quek, K. P. Loh, *Nat. Chem.* **2017**, *9*, 563-570; c) M. T. Manzari, Y. Shamay, H. Kiguchi, N. Rosen, M. Scaltriti, D. A. Heller, *Nat. Rev. Mater.* **2021**, *6*, 351-370.

[2] a) M. A. Rahim, N. Jan, S. Khan, H. Shah, A. Madni, A. Khan, A. Jabar, S. Khan, A. Elhissi, Z. Hussain, H. C. Aziz, M. Sohail, M. Khan, H. E. Thu, *Cancers* **2021**, *13*, 670; b) S. Municoy, M. I. Alvarez Echazu, P. E. Antezana, J. M. Galdoporpora, C. Olivetti, A. M. Mebert, M. L. Foglia, M. V. Tuttolomondo, G. S. Alvarez, J. G. Hardy, M. F. Desimone, *Int. J. Mol. Sci.* **2020**, *21*, 4724; c) Y. Zhang, C. Xu, X. Yang, K. Pu, *Adv. Mater.* **2020**, *32*, 2002661; d) M. Kang, Z. Zhang, N. Song, M. Li, P. Sun, X. Chen, D. Wang, B. Z. Tang, *Aggregate* **2020**, *1*, 80-106; e) J. Hu, W. Jiang, L. Yuan, C. Duan, Q. Yuan, Z. Long, X. Lou, F. Xia, *Aggregate* **2021**, *2*, 48-56.

[3] a) S. Bonnet, *Dalton Trans.* **2018**, *47*, 10330-10343; b) F. Zhang, Q. Wu, H. Liu, *WIREs Nanomed. Nanobiotechnol.* **2020**, *12*, e1643; c) A. Presa, G. Vazquez, L. A.

Barrios, O. Roubeau, L. Korrodi-Gregorio, R. Perez-Tomas, P. Gamez, *Inorg. Chem.* **2018**, *57*, 4009-4022; d) C. Matera, A. M. J. Gomila, N. Camarero, M. Libergoli, C. Soler, P. Gorostiza, *J. Am. Chem. Soc.* **2018**, *140*, 15764-15773; e) F. Reessing, W. Szymanski, *Curr. Med. Chem.* **2017**, *24*, 4905-4950; f) J. A. Cuello-Garibo, M. S. Meijer, S. Bonnet, *Chem. Commun.* **2017**, *53*, 6768-6771; g) C. Mari, V. Pierroz, A. Leonidova, S. Ferrari, G. Gasser, *Eur. J. Inorg. Chem.* **2015**, 3879-3891; h) Y. Chen, W. Lei, G. Jiang, Y. Hou, C. Li, B. Zhang, Q. Zhou, X. Wang, *Dalton Trans.* **2014**, *43*, 15375-15384.

[4] a) Z. Wang, N. Wang, S.-C. Cheng, K. Xu, Z. Deng, S. Chen, Z. Xu, K. Xie, M.-K. Tse, P. Shi, H. Hirao, C.-C. Ko, G. Zhu, *Chem* **2019**, *5*, 3151-3165; b) V. H. S. van Rixel, V. Ramu, A. B. Auyeung, N. Beztsinna, D. Y. Leger, L. N. Lameijer, S. T. Hilt, S. E. Le Devedec, T. Yildiz, T. Betancourt, M. B. Gildner, T. W. Hudnall, V. Sol, B. Liagre, A. Kornienko, S. Bonnet, *J. Am. Chem. Soc.* **2019**, *141*, 18444-18454; c) P. Klan, T. Solomek, C. G. Bochet, A. Blanc, R. Givens, M. Rubina, V. Popik, A. Kostikov, J. Wirz, *Chem. Rev.* **2013**, *113*, 119-191.

[5] a) Z. Du, C. Liu, H. Song, P. Scott, Z. Liu, J. Ren, X. Qu, *Chem* **2020**, *6*, 2060-2072; b) F. Wang, Y. Zhang, Z. Du, J. Ren, X. Qu, *Nat. Commun.* **2018**, *9*, 1209; c) G. Y. Tonga, Y. Jeong, B. Duncan, T. Mizuhara, R. Mout, R. Das, S. T. Kim, Y.-C. Yeh, B. Yan, S. Hou, V. M. Rotello, *Nat. Chem.* **2015**, *7*, 597-603; d) T. Voelker, F. Dempwolff, P. L. Graumann, E. Meggers, *Angew. Chem., Int. Ed.* **2014**, *53*, 10536-10540; e) J. G. Rebelein, T. R. Ward, *Curr. Opin. Biotechnol.* **2018**, *53*, 106-114; f) D. M. Patterson, L. A. Nazarova, J. A. Prescher, *ACS Chem. Biol.* **2014**, *9*, 592-605.

[6] a) M. Darguzyte, R. Holm, J. Baier, N. Drude, J. Schultze, K. Koynov, D. Schwiertz, S. M. Dadfar, T. Lammers, M. Barz, F. Kiessling, *Bioconjugate Chem.* **2020**, *31*, 2691-2696; b) M. Darguzyte, N. Drude, T. Lammers, F. Kiessling, *Cancers* **2020**, *12*, 295; c) Y. Tsvetkova, N. Beztsinna, M. Baues, D. Klein, A. Rix, S. K. Golombek, W.

Al Rawashdeh, F. Gremse, M. Barz, K. Koynov, S. Banala, W. Lederle, T. Lammers, F. Kiessling, *Nano Lett.* **2017**, *17*, 4665-4674; d) S. Pal, C. Dalal, N. R. Jana, *ACS Omega* **2017**, *2*, 8948-8958; e) N. Beztsinna, Y. Tsvetkova, M. Bartneck, T. Lammers, F. Kiessling, I. Bestel, *Bioconjugate Chem.* **2016**, *27*, 2048-2061.

[7] a) L. Xu, X. Liang, S. Zhang, B. Wang, S. Zhong, M. Wang, X. Cui, *Dyes Pigm.* **2020**, *182*, 108642; b) B. König, S. Kümmel, E. Svobodová, R. Cibulka, *Phys. Sci. Rev.* **2018**, *3*, 20170168; c) G. de Gonzalo, M. W. Fraaije, *ChemCatChem.* **2013**, *5*, 403-415; d) S. Bloom, C. Liu, D. K. Kolmel, J. X. Qiao, Y. Zhang, M. A. Poss, W. R. Ewing, D. W. C. MacMillan, *Nat. Chem.* **2018**, *10*, 205-211.

[8] a) S. Alonso-de Castro, A. L. Cortajarena, F. Lopez-Gallego, L. Salassa, *Angew. Chem., Int. Ed.* **2018**, *57*, 3143-3147. b) R. Zhang, X. Song, Y. Liu, P. Wang, Z. Wang, Z. Zheng, Y. Dai, B. Huang, *J. Mater. Chem. A* **2019**, *7*, 26934-26943.

[9] a) X. Ling, L. Huang, Y. Li, Q. Wan, Z. Wang, A. Qin, M. Gao, B. Z. Tang, *Mater. Horiz.* **2020**, *7*, 2696-2701; b) S. Li, X. Ling, Y. Lin, A. Qin, M. Gao, B. Z. Tang, *Chem. Sci.* **2018**, *9*, 5730-5735.

[10] a) D. S. Benoit, H. Koo, *Nanomedicine.* **2016**, *11*, 873-879; b) M. Upreti, A. Jyoti, P. Sethi, *Transl. Cancer Res.* **2013**, *2*, 309-319; c) S. Thakkar, D. Sharma, K. Kalia, R. K. Tekade, *Acta Biomater.* **2020**, *101*, 43-68; d) Y.-L. Su, T.-W. Yu, W.-H. Chiang, H.-C. Chiu, C.-H. Chang, C.-S. Chiang, S.-H. Hu, *Adv. Funct. Mater.* **2017**, *27*, 1700056.

[11] a) L. Crovetto, V. Martinez-Junza, S. E. Braslavsky, *Photochem. Photobiol.* **2006**, *82*, 281-290; b) C. Feldmeier, H. Bartling, K. Magerl, R. M. Gschwind, *Angew. Chem., Int. Ed.* **2015**, *54*, 1347-1351; c) T. Langenbacher, D. Immeln, B. Dick, T. Kottke, *J. Am. Chem. Soc.* **2009**, *131*, 14274-14280; d) U. Megerle, M. Wenninger, R. J. Kutta, R. Lechner, B. Konig, B. Dick, E. Riedle, *Phys. Chem. Chem. Phys.* **2011**, *13*, 8869-8880.

[12] a) D. R. Cardoso, K. Olsen, L. H. Skibsted, *J. Agric. Food Chem.* **2007**, *55*, 6285-6291; b) N. K. Hall, T. M. Chapman, H. J. Kim, D. B. Min, *Food Chem.* **2010**, *118*, 534-539; c) R. Shimizu, M. Yagi, A. Kikuchi, *J. Photochem. Photobiol., B* **2019**, *191*, 116-122.

[13] a) S. Alonso-de Castro, E. Ruggiero, A. Ruiz-de-Angulo, E. Rezabal, J. C. Mareque-Rivas, X. Lopez, F. Lopez-Gallego, L. Salassa, *Chem. Sci.* **2017**, *8*, 4619-4625; b) D. R. Cardoso, S. H. Libardi, L. H. Skibsted, *Food Funct.* **2012**, 3, 487-502; c) K. A. Korvinson, G. N. Hargenrader, J. Stevanovic, Y. Xie, J. Joseph, V. Maslak, C. M. Hadad, K. D. Glusac, *J. Phys. Chem. A* **2016**, *120*, 7294-7300.

[14] a) S. Kumar, M. S. Tomar, A. Acharya, *Leuk. Lymphoma* **2015**, *56*, 1846-1855; b) K. F. Wan, S. L. Chan, S. K. Sukumaran, M. C. Lee, V. C. Yu, *J. Biol. Chem.* **2008**, *283*, 8423-8433; c) Y. Zhang, P. Murugesan, K. Huang, H. Cai, *Nat. Rev. Cardiol.* **2020**, *17*, 170-194; d) G. R. Drummond, S. Selemidis, K. K. Griendling, C. G. Sobey, *Nat. Rev. Drug Discovery* **2011**, *10*, 453-471.

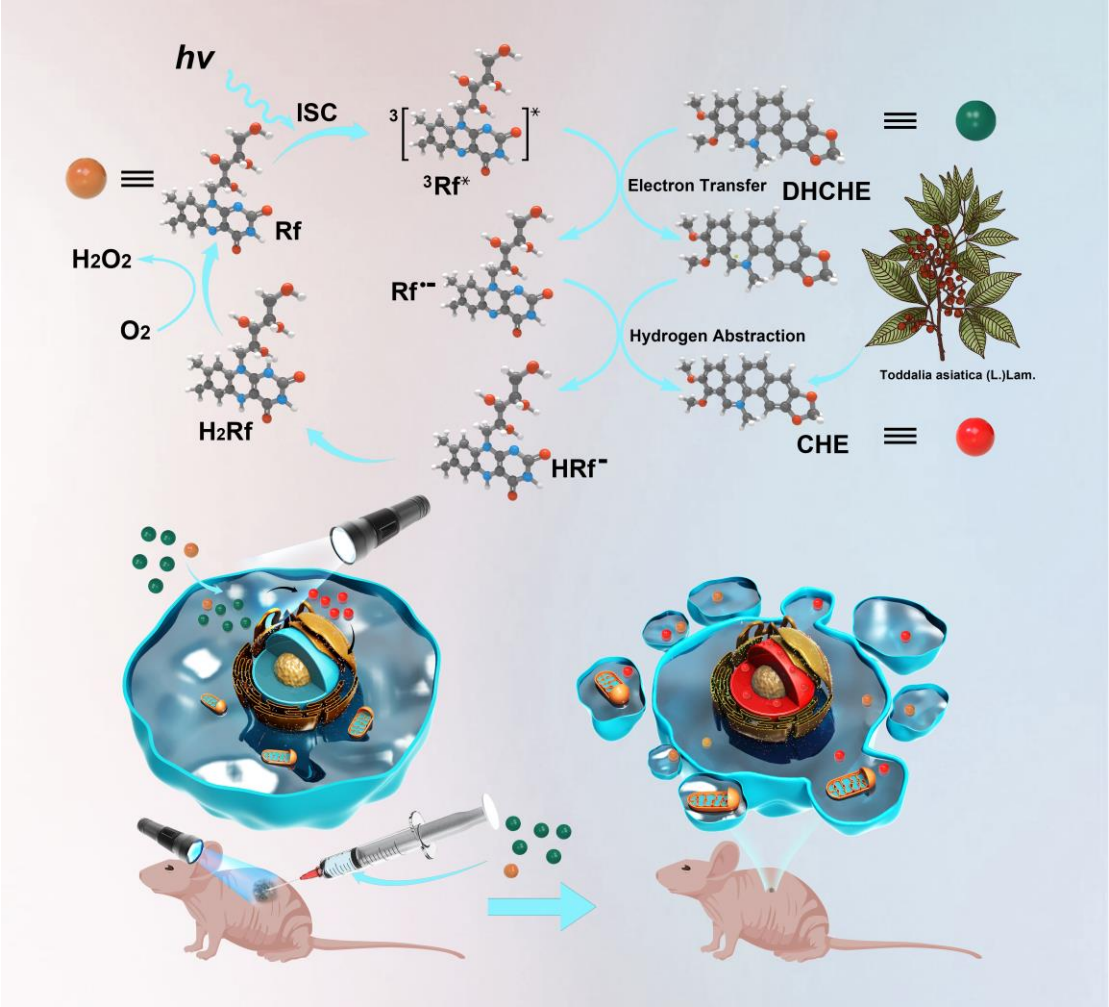

Scheme 1. Schematic illustration of photo-catalytic transformation of prodrug DHCHE into anti-cancer drug CHE with riboflavin as the bioorthogonal photocatalyst.

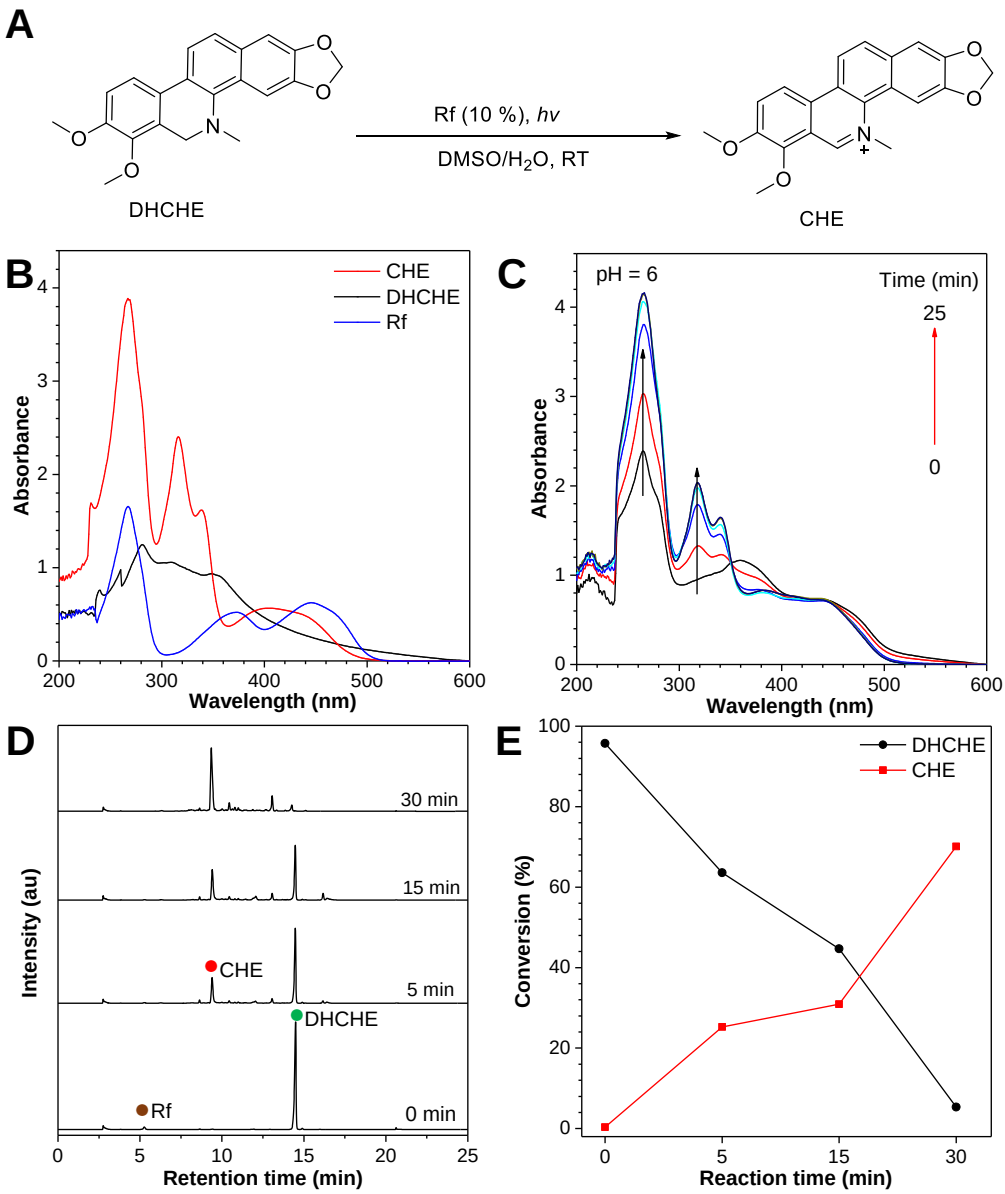

Figure 1. A) The photooxidative transformation from DHCHE into CHE promoted by riboflavin (Rf) in solution of DMSO/water (v : v = 10 : 90). B) Absorption spectra of DHCHE, CHE and Rf in Britton-Robinson buffer solution (pH = 6, DMSO/water (v : v = 10: 90)). [DHCHE] = 100 μM, [CHE] = 100 μM, [Rf] = 50 μM. C) UV-Vis absorption spectra of "DHCHE + Rf" in Britton-Robinson buffer solution (pH = 6, DMSO/water (v : v = 10 : 90)) under white light irradiation (34 mW cm^{-2}). [DHCHE] = 100 μM, [Rf] = 50 μM; D E) Time-dependent HPLC spectra and conversion ratio of DHCHE in the presence of Rf under blue light irradiation (500 nm, 50 mW cm^{-2}) ([DHCHE] = 0.5 mg mL^{-1}, [Rf] = 0.05 mg mL^{-1}). ● CHE, ● DHCHE and ● Rf.

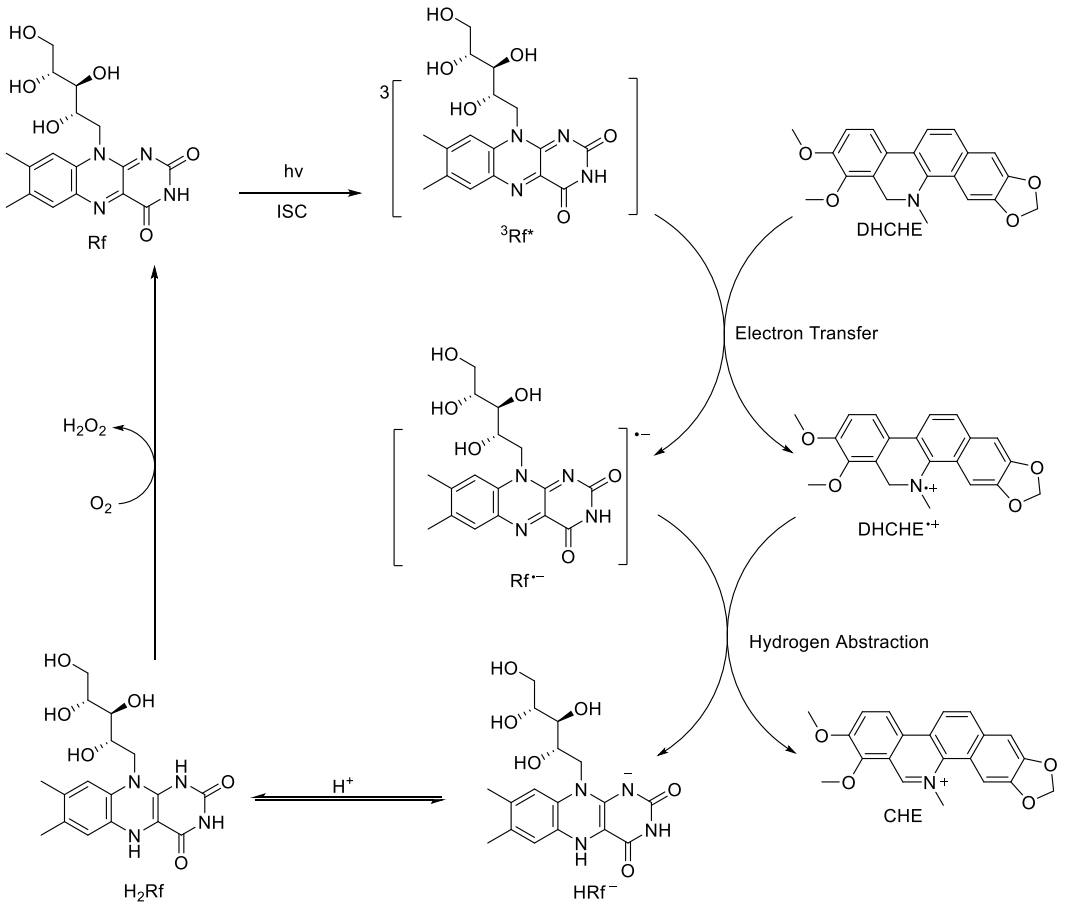

Scheme 2. The proposed reaction mechanism for catalyzed transformation from DHCHE into CHE with riboflavin as the photocatalyst.

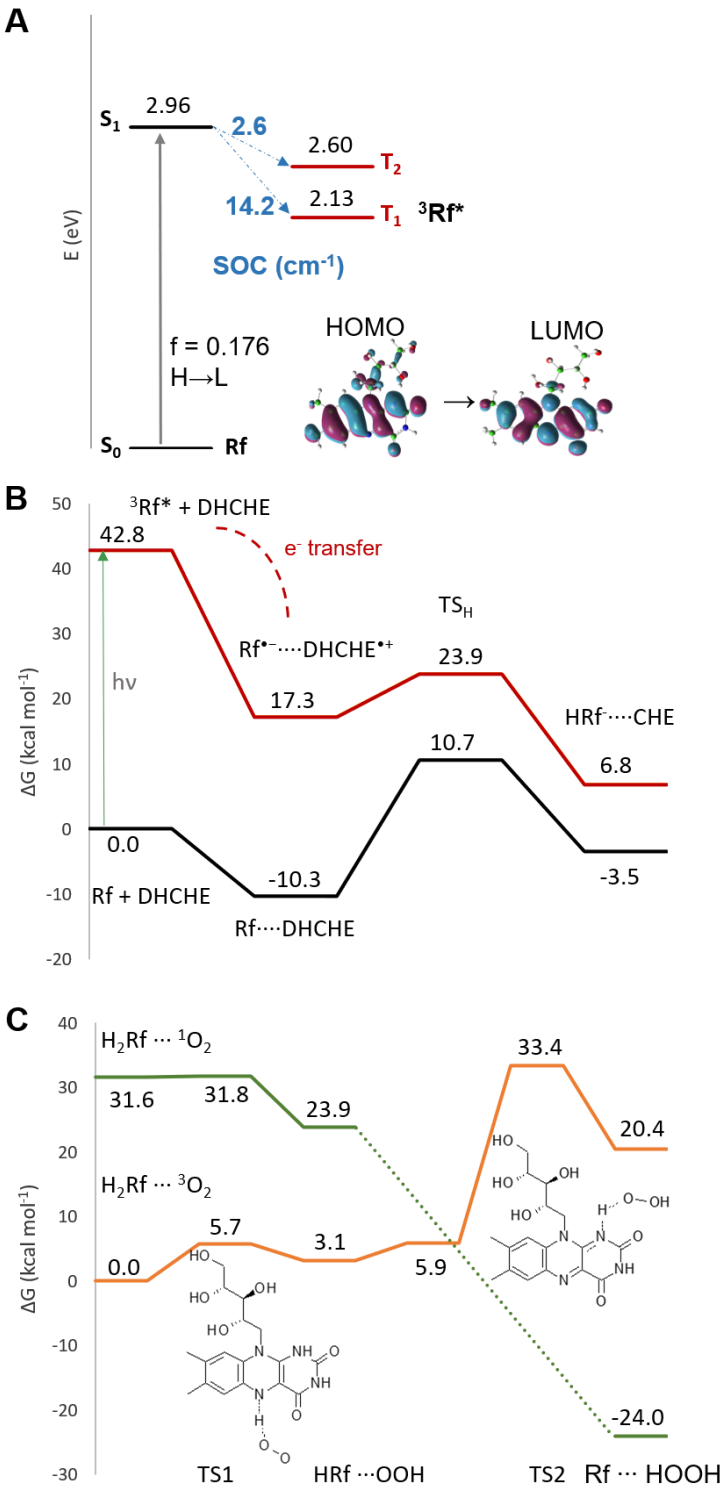

Figure 2. Outcomes of computational exploration: A) photophysical behaviour of Rf, including excitation energies (eV) of the potentially involved states, SOC (cm^{-1}) between them and HOMO and LUMO plots; B) free energy profile for Rf + DHCHE reaction leading to CHE production along the excited triplet (red line) and ground (black line) states of Rf (relative energies were calculated with respect to the sum of the energies of Rf in its ground state and DHCHE as reference; C) free energy profile for H_2Rf conversion to Rf along triplet (orange line) and singlet (green line) surfaces, the relative energies were calculated considering the sum of H_2Rf and ground state of oxygen ($^3O_2$) energies as reference.

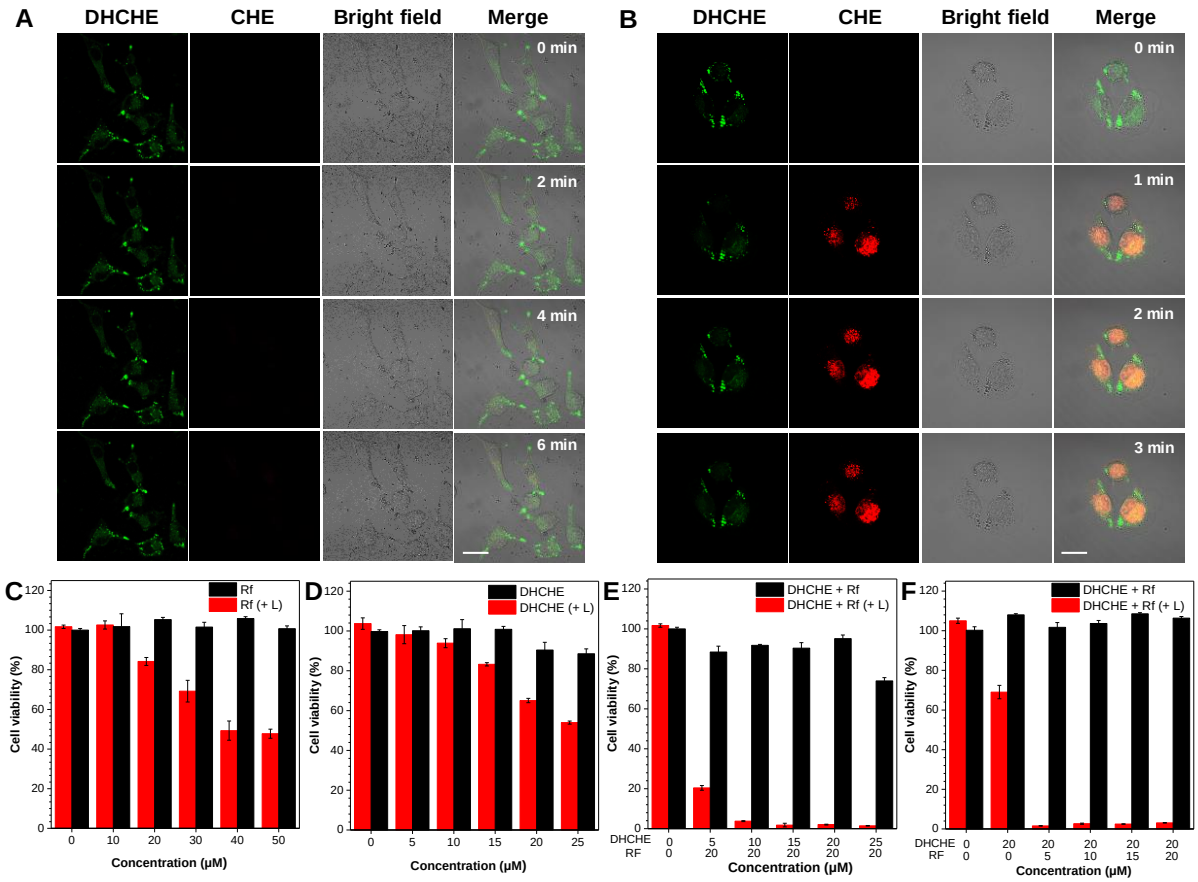

Figure 3. A B) Time-dependent CLSM images of A375 cells respectively incubated with DHCHE, "DHCHE + Rf" under white light irradiation (34 mW cm^{-2}). [DHCHE] = 50 μM, [Rf] = 10 μM. For DHCHE (green channel), λ_{ex} = 405 nm, λ_{em} = 420-520 nm. For CHE (red channel), λ_{ex} = 488 nm, λ_{em} = 580-700 nm. Scale bar = 20 μm. C-F) Cytotoxicity of A375 cells by treatment with Rf, DHCHE and "DHCHE + Rf" at different concentration under dark and white light irradiation (34 mW cm^{-2}) for 10 min.

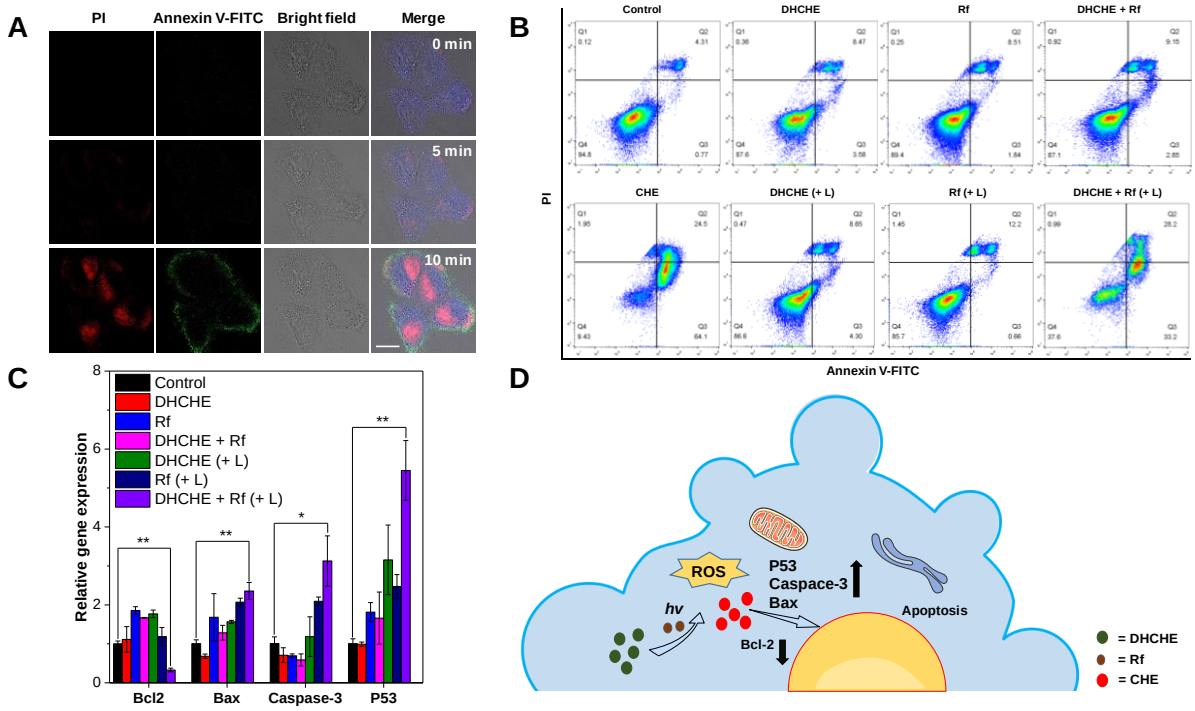

Figure 4. A) CLSM images of A375 cells treated with "DHCHE + Rf" and futher stained with Annexin V-FITC/PI. [DHCHE] = 50 μM, [Rf] = 10 μM. For Annexin V-FITC, λ_{ex} = 488 nm, λ_{em} = 510-550 nm. For PI, λ_{ex} = 543 nm, λ_{em} = 560-625 nm. Scale bar = 20 μm. B) Flow cytometric analysis of A375 cells treated with DHCHE, Rf, "DHCHE + Rf (+ L)" under dark or white light irradiation (34 mW cm^{-2}) for 10 min. C) Gene expression levels of the pro-apoptotic (Bax, Caspase-3 and P53) and anti-apoptotic gene (Bcl2) analyzed by qRT-PCR. Expression levels were normalized to expression levels in control group cells. Bars with different characters are statistically different at *p < 0.05, **p < 0.01 versus control. D) Schematic illustration of bioorthogonal photocatalyzed cancer chemotherapy strategy.

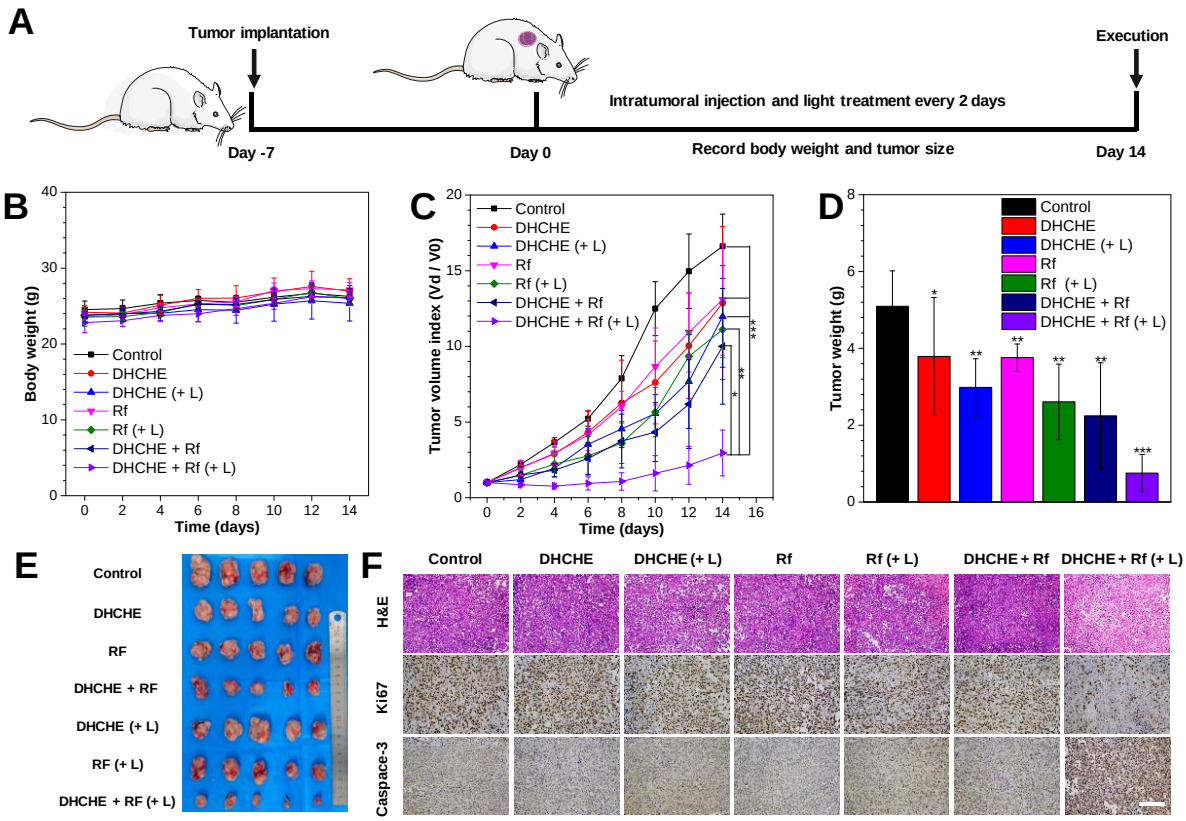

Figure 5. A) Schematic diagram of A375 tumor-bearing mice model development and treatment process. B) The body weight of tumor-bearing mice under control and treatment with DHCHE, DHCHE (+ L), Rf, Rf (+ L), "DHCHE + Rf", "DHCHE + Rf (+ L)", respectively. C) the tumor volume index of tumor-bearing mice after different treatments for 14 d. (Data are given as mean ± standard deviation (SD), n = 5, **p < 0.01, ***p < 0.001). D) The average tumor weight of tumor-bearing mice under control and treatment with DHCHE, DHCHE (+ L), Rf, Rf (+ L), "DHCHE + Rf", "DHCHE + Rf (+ L)", respectively. Bars with different characters are statistically different at *p < 0.05, **p < 0.01, ***p < 0.001 versus control. E) The photographs of tumors collected from different groups of A375 tumor-bearing mice at day 14. F) Representative images of H&E, Ki67 and Caspace-3 staining from tumor sections after the indicated treatments.

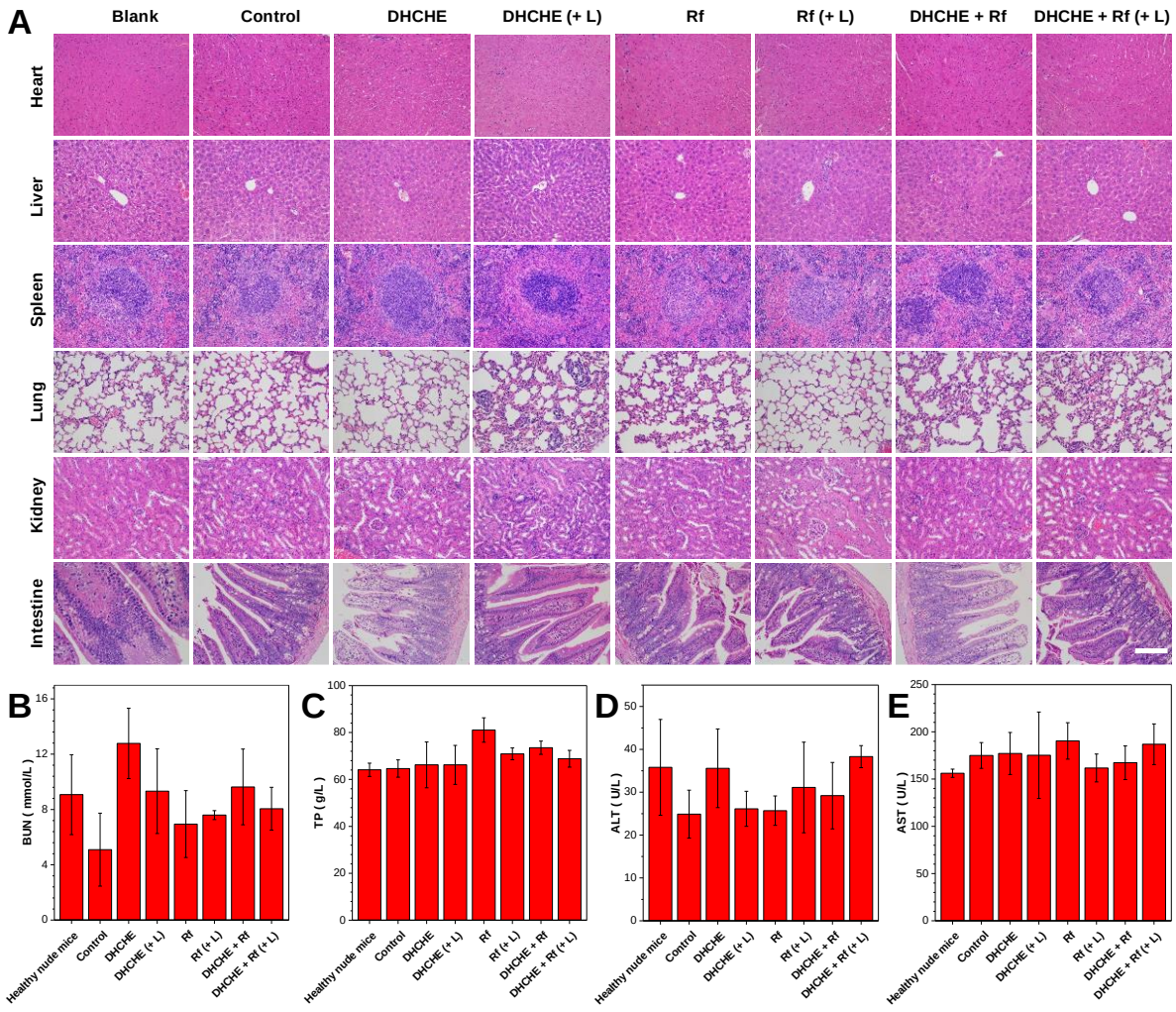

Figure 6. A) H&E staining of the major organs sections from healthy mice and A375 bearing mice at day 14 under blank (healthy nude mice), control and treatment with DHCHE, DHCHE (+ L), Rf, Rf (+ L), "DHCHE + Rf", "DHCHE + Rf (+ L)", respectively. Scale bar = 100 μm. B-E) Blood biochemistry indices of BUN, TP, ALT, AST. (Data are given as mean ± standard deviation (SD), n = 3).

TOC

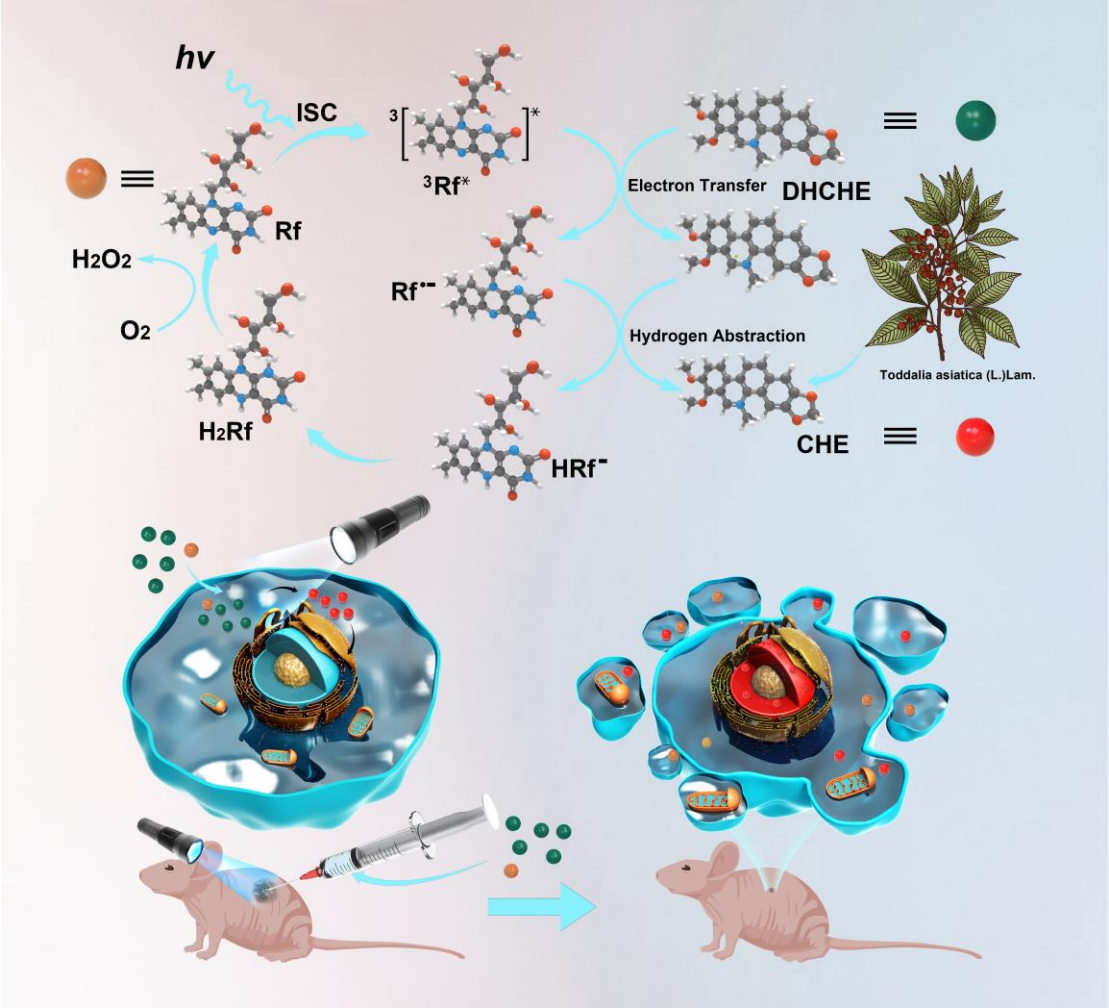
hv
ISC
Rf
H2O2
O2
H2Rf
3Rf*
Rf•−
HRf−
Electron Transfer
DHCHE
Hydrogen Abstraction
CHE
Toddalia asiatica (L.)Lam.